# Spectroscopic and structural studies of isochronally annealed cobalt oxide nanoparticles

**ARTICLE** *in* JOURNAL OF PHYSICS AND CHEMISTRY OF SOLIDS · DECEMBER 2013

Impact Factor: 1.85 · DOI: 10.1016/j.jpcs.2013.11.010

Journal of Physics and Chemistry of Solids 75 (2014) 397–402

Contents lists available at ScienceDirect

Journal of Physics and Chemistry of Solids

journal homepage: www.elsevier.com/locate/jpcs

# Spectroscopic and structural studies of isochronally annealed cobalt oxide nanoparticles

Harishchandra Singh [a], A.K. Sinha [a,*], M.N. Singh [a], P. Tiwari [a], D.M. Phase [b], S.K. Deb [a]

[a] Indus Synchrotron Utilization Division, Raja Ramanna Centre for Advanced Technology, Indore 452013, India
[b] UGC DAE Consortium for Scientific Research, Indore 452010, India

ARTICLE INFO

*Article history:*
Received 3 September 2013
Received in revised form
24 October 2013
Accepted 18 November 2013
Available online 1 December 2013

*Keywords:*
A. Cobalt oxide nanoparticles
C. XANES
C. Photoelectron spectroscopy
C. X-ray diffraction
D. Crystal fields

ABSTRACT

X-ray absorption near edge structure (XANES) spectroscopy, X-ray photoelectron spectroscopy (XPS), and Synchrotron X-ray diffraction (SXRD) techniques are used to study as synthesized and isochronally annealed samples of cobalt oxide nanoparticles (NPs) grown using the wet chemical route. Quantitative phase composition determined using Linear Combination Fitting (LCF) on XANES data is found to be in reasonably good agreement with that obtained from Rietveld refinement on SXRD data. XPS data qualitatively indicate that $Co_3O_4$ concentration increases with increase in the annealing temperature, in confirmation with SXRD and XANES data. Larger shifts in the satellite peaks from the main peaks compared to these in bulk suggest larger crystal field splitting in nanoparticles as compared to the bulk.


## 1. Introduction

Mixed oxidation state of transition metal oxides (TMO) is the root cause of unusual physical, chemical and magnetic properties [1]. This makes the study of mixed oxidation state of TMOs important from fundamental as well as application point of view. For example, cobalt oxide nanoparticles (NPs) have wide range of applications such as catalytic oxidation of carbon monoxide (CO) [2], water oxidation under mild conditions [3], magnetic materials [4], electro chromic devices [5], high temperature solar selective absorber [6] and gas sensors [7] etc. Magnetic NPs also have biomedical applications such as drug delivery and contrast enhancement agents for magnetic resonance imaging (MRI) [8]. The spinel structure of cobalt oxide ($Co_3O_4$) can act as an efficient catalyst in the heterogeneous chemical processes [9]. Cobalt oxides are formed in five different oxidation states of Co. $CoO_2$, $Co_2O_3$, CoO (OH), CoO and $Co_3O_4$ are the oxides of Co with different oxidation states. Out of these, $Co_3O_4$ (oxidation state +8/3) and CoO (Oxidation state +2) are stable oxides. Bulk $Co_3O_4$ has a cubic spinel structure in which the $Co^{2+}$ ions occupy the tetrahedral (8*a*) site whereas $Co^{3+}$ ions at octahedral (16*d*) one [10]. $Co^{3+}$ ions are in a diamagnetic $t_{2g}^6$ (low spin, $S=0$) state due to strong octahedral cubic field and large crystal-field splitting between $t_{2g}$ and $e_g$ levels in the 3d orbitals, while $Co^{2+}$ ions at the 8*a* site are in a high spin state $e_g^4\ t_{2g}^3$ with $S=3/2$. As a result, $Co^{3+}$ ions are not magnetic and the antiferromagnetism posses by $Co_3O_4$ are mainly due to the weak coupling between nearest neighbor $Co^{2+}$ ions [10]. Bulk CoO is also antiferromagnetic in nature and it has simple cubic structure in which $Co^{2+}$ ions occupy the octahedral site.

In this paper, spectroscopic and structural investigation of mixed oxidation states on as grown as well as isochronally annealed cobalt oxide NPs samples are carried out. Spectroscopic method (e.g. X-ray absorption spectroscopy (XAS)) generally measures the response of a system as a function of energy. X-ray absorption near edge structure (XANES) spectroscopy and X-ray photoelectron spectroscopy (XPS) are two spectroscopic tools which are sensitive to bulk and surface of the samples respectively. Information obtained are also complementary in the sense that XPS gives information about occupied density of states (DOS) below the Fermi level, whereas XANES that for unoccupied DOS just above the Fermi level. In XANES spectra, features such as K-edge, pre-edge and near edge provide detailed information on the oxidation state, the coordination environment and the unoccupied DOS respectively. However, the information on the coordination environment is an average of various possible coordination. In XPS, main peak positions, peak separation and position of other special features like shake up satellites are used for classification of different chemical states of an element in that particular sample. Herein, Rietveld refinement on powder SXRD data are carried out to obtain the composition of mixed phase samples and their lattice parameters. The composition analysis has also been done using Linear Combination Fitting (LCF) on XANES data. Quantitative approach used in XANES experiments is based on statistical

* Correspondence to: Indus Synchrotron Utilization Division, RRCAT, Room no. 25, Indus-2 Building, Indore 452013, India. Tel.: +91 731 2442125; fax: +91 731 2442140.
*E-mail address:* anil@rrcat.gov.in (A.K. Sinha).

0022-3697/$ - see front matter © 2013 Elsevier Ltd. All rights reserved.
http://dx.doi.org/10.1016/j.jpcs.2013.11.010

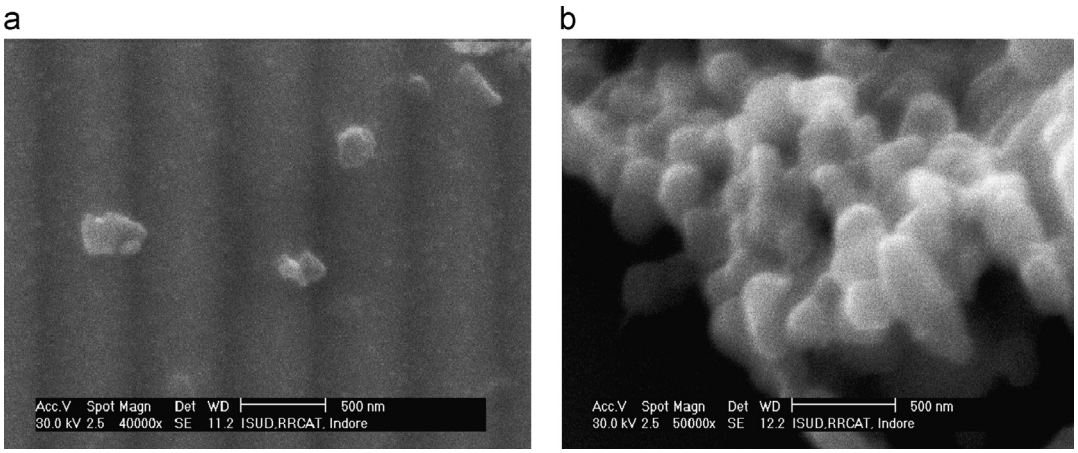


**Fig. 1.** SEM image of two samples (a) H1 and (b) H4.

goodness-of-fit and does not explain the accuracy of the components obtained from the LCF fittings [11]. In this work, we show that a good agreement between the composition obtained from the XRD and XANES ensures the validity of LCF on XANES data.

## 2. Experimental

Cobalt oxide nanoparticles were synthesized using the wet chemical route. The reactants used were cobalt nitrate $Co(NO_3)_2 \cdot 6H_2O$ as a precursor, 2-pyrrolidone as solvent, oleic acid and trioctylphosphine oxide (TOPO) as surfactants. The chemicals used were of analytical grade and were procured from Sigma Aldrich. 0.5 g (1.72 mM) $Co(No_3)_2 \cdot 6H_2O$ was dissolved in 25 mL (0.33 M) 2-pyrrolidone. 2 mL (6.2 mM) oleic acid and 2.4 g (6.2 mM) trioctylphosphine oxide were mixed with the above solution at 50 °C and stirred for 30 min. The reaction took place in two steps. After heating at 50 °C and stirring the mixture for ~30 min, the solution changed to transparent pink color. This indicates the completion of the first phase. The solution was heated in air at 200 °C for 1 h and a black solution was observed. The solution was then cooled to the room temperature and diluted with methanol. Black powder was separated from the solution using centrifuge. The powder was dried at 65 °C for about 10 h in the oven. More details of the synthesis are given elsewhere [12]. For this work, the synthesis is done at higher temperature (280 °C) and for longer time compared to that reported in our earlier work [12]. The base sample (as grown) was further annealed at various temperatures from 300 °C to 800 °C for ~2 h in air. We have chosen four samples (1) H1: as grown, (2) H2: annealed at 300 °C for 2 h, (3) H3: annealed at 500 °C for 2 h, and (4) H4: annealed at 800 °C for 2 h for spectroscopic and structural studies. Obtained samples were characterized using scanning electron microscopy (SEM) to investigate the typical size of nanoparticle. SEM images were obtained using Phillips microscope (model XL30CP, 30KV). For SEM measurements, NPs were dispersed in methanol and were ultrasonicated for 15 min. These particles were dispersed dropwise on cleaned Si wafer. The samples were then dried under lamp light. A 100 Å thick gold layer was deposited on the samples to nullify the charging effect while performing SEM. Spectroscopic and structural studies have been done using the XANES, XPS and SXRD techniques. XPS measurements were performed at room temperature with an OMICRON 180° hemispherical analyzer (model EA 125) using Al Kα (photon energy = 1486.7 eV) source [13]. The hemispherical analyzer was operated in constant-pass energy mode and its overall energy resolution with pass energy of 50 eV was estimated to be 0.8 eV. The measurements were carried out with a photoelectron take-off angle of 45° and the pressure in the spectrometer chamber during the measurements was $\sim 10^{-10}$ mbar. XANES and SXRD measurements were performed at angle dispersive X-ray diffraction (ADXRD) beamline (BL-12) [14] on Indus-2 synchrotron source [15]. The beamline consists of a Si (111) based double crystal monochromator and two experimental stations namely a six circle diffractometer with a scintillation point detector and Mar 345 dtb image plate area detector. SXRD measurements were carried out using the image plate. The X-ray wave length used for the present study was accurately calibrated by doing X-ray diffraction on $LaB_6$ NIST standard. Data reductions were done using Fit2D software [16]. XANES measurements were carried out in transmission mode at room temperature. Absorption by the samples was measured by measuring incident intensity before and transmitted intensity after the sample using two ionization chambers around the Co K-edge (7.709 keV). Photon energy was calibrated by measuring the XANES spectra of standard cobalt metal at Co K-edge. Energy resolution ($\Delta E/E$) and energy reproducibility were estimated to be $1.5 \times 10^{-4}$ and 0.2 eV respectively.

## 3. Results and discussion

### 3.1. Scanning electron microscopy (SEM)

Fig. 1a and b shows SEM images for as grown (H1) and sample annealed at 800 °C (H4) respectively. The average size of the particle is ~180 nm (Fig. 1b). SEM image shows that annealing has lead to the coalescence of nanoparticles (Fig. 1b). In case of as grown sample and sample annealed at 300 °C, weak type II magnetic contrast is seen due to the some leakage field above the cobalt nanoparticles surface. This also verifies the Rietveld refinement result which shows the presence of Co metallic nanoparticle phase in two samples H1 and H2 (to be discussed in Section 3.4).

### 3.2. XANES

XANES spectroscopy is an element specific technique and is highly sensitive to the oxidation state, local coordination and hybridization effects of orbitals of that specific element. Generally XANES measurements (where absorption edge is being probed) are performed to study oxidation state, local surroundings and electronic states of specific metal site [17–19]. However in this work, XANES measurements on all the samples have been performed to investigate the composition of mixed phase. Fig. 2 shows the normalized Co K-edge XANES spectra of nanoparticles

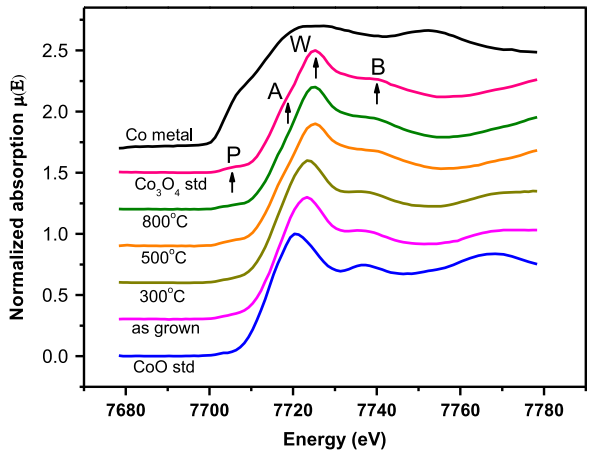


**Fig. 2.** Normalized Co K-edge XANES spectra for all the samples H1–H4, along with CoO (H0) and $Co_3O_4$ (H5) standards. Vertical shifting has been done for the sake of clarity. Features in the XANES spectra are marked with P (Pre-edge), A (Main edge), W (White line) and B. Energy calibration has been done using Co metal foil XANES spectra.

samples H1–H4 and two standard samples CoO (H0) and $Co_3O_4$ (H5) with known oxidation states of Co. As shown in Fig. 2, XANES spectrum is divided into four parts namely the pre-edge (marked 'P'), the main edge (marked 'A'), white line (marked 'W') and the extended edge region (marked 'B'). All these regions correspond to different transition energies observed for that particular element in the compound. The pre-edge corresponds to 1s→3d transition, a dipole forbidden (quadrupole) transition is allowed because of favored co-ordination environment of the absorbing atom. For example, $Co^{3+}$ in octahedral oxygen cage gives rise to significant 1s→3d transition. Intensity of the pre-edge gives information about the coordination geometry of transition metal site like tetrahedral and/or octahedral oxygen cage [20]. The main edge is attributed to 1s→4s monopole transition, whereas the white line corresponds to dipole allowed 1s→4p transition [21,22]. Main edge (rising edge) gives information about the oxidation state of the absorbing atom in the sample. This edge position shifts when the effective number of positive charges i.e. oxidation state changes resulting from 1s core hole shielding effects. In a sample with mixed oxidation state, the main edge is located in between the edge positions of the two. Using the Linear Combination Fitting (LCF) technique one can quantitatively estimate the concentrations of the two phases in the sample.

A detailed qualitative as well as quantitative (using software Athena [23]) XANES analysis has been done. For the analysis, we have used XANES spectra of two standard samples CoO and $Co_3O_4$ along with Co metal foil to calibrate the photon energy (Fig. 2). Quantitative phase composition analysis has been done using the LCF method [11,24]. The position of main edge in XANES spectra for all the samples has been determined by the energy corresponding to ~0.5 absorptions in the normalized XANES spectra. XANES spectrum of sample H0 (CoO) shows a minor pre-edge peak (Fig. 2), which signifies octahedral configuration of O around Co in agreement with the literature [25]. On the other hand, significant pre-edge peak is observed for standard sample H5 ($Co_3O_4$) and is attributed to tetrahedral configuration of O around Co [25]. This makes dipole forbidden 1s→3d (quadrupole) transition possible with the mixing of O 2p and Co 3d orbitals. Here, a visible pre-edge feature for sample H1 is observed. Further, the intensity of the pre-edge becomes more prominent with the increase in the annealing temperatures. In addition, for samples H1–H4 the energy positions of the main edge peak (marked A, Fig. 2) shifts towards higher energies with the increase in the annealing temperature. Both these observations indicate increase in $Co_3O_4$ concentration on raising the annealing temperature [25]. We have summarized energy positions of 1s→3d, 1s→4s and 1s→4p transitions along with energy differences between 3d→4s, 3d→4p and 4s→4p transitions for all the samples H0–H5 in Table 1. For the two standard oxides, the main edge transition energy for $Co_3O_4$ is blue shifted ~3.7 eV as compared to CoO. The main edge energies of the NP samples H1–H3 are found to be intermediate between the two standard oxide samples, whereas that of sample H4 is the same as that of $Co_3O_4$. This indicates mixed phase behavior of samples H1–H3 as compared to H4. White line positions for the standard samples indicate that $Co_3O_4$ peak is also blue shifted (~4.9 eV) with respect to the CoO (Table 1). Feature which is marked as B (extended edge region) occurs due to the surrounding environment. This feature is similar in the samples H3, H4 and H5 suggesting almost similar kind of surrounding environment for sample H3 and H4 as compared to standard H5. Whereas, the same feature for sample H0 is quite sharp. This indicates different kind of environment for Co in the sample H0 as compared to samples H3 and H4. The same feature for samples H1 and H2 are intermediate. We conclude from the above analysis that as grown sample together with sample annealed at 300 °C are in the mixed phases of CoO and $Co_3O_4$. All these observations indicate that annealing at higher temperatures lead to the transformation of CoO to $Co_3O_4$ phase [26]. A sharp jump of $Co_3O_4$ concentration is observed in Table 2 for 500 °C compared with 300 °C. Oxidation of Co metallic phase to CoO or $Co_3O_4$ is a two step process. First step corresponds to transition from Co to CoO and second one is from CoO to $Co_3O_4$ [26]. Atomic structural changes and diffusion processes during the chemical transformation of Co NPs to CoO NPs and then $Co_3O_4$ has also been reported [26]. CoO stabilizes via O in-diffusion by an indirect exchange mechanism through interstitial O and vacancies of certain type of Co sites from Co metallic NP phase. For $Co_3O_4$,

**Table 1**
Electronic transition energies and their differences are tabulated for all the samples H0–H5.

| Samples | Transition energies (eV) | | | $\Delta E$ (eV) | | |
|---|---|---|---|---|---|---|
| | 1s–3d | 1s–4s | 1s–4p | 3d–4s | 3d–4p | 4s–4p |
| CoO | 7703.05 | 7713.56 | 7720.36 | 10.51 | 17.31 | 6.80 |
| As grown | 7703.70 | 7715.59 | 7723.21 | 11.89 | 19.51 | 7.62 |
| 300 °C | 7703.89 | 7715.85 | 7723.43 | 11.96 | 19.54 | 7.58 |
| 500 °C | 7704.49 | 7716.66 | 7725.26 | 12.17 | 20.77 | 8.60 |
| 800 °C | 7704.64 | 7717.27 | 7725.29 | 12.63 | 20.65 | 8.02 |
| $Co_3O_4$ | 7704.63 | 7717.26 | 7725.28 | 12.63 | 20.65 | 8.02 |

**Table 2**
Phase compositions obtained from Rietveld refinement on SXRD data and LCF on XANES data of cobalt oxide nanoparticles samples H1–H4 are tabulated, along with refined cell parameters.

| Sample no. | Annealing temp (°C) | Phases present | Composition obtained | | Cell parameter (Å) |
|---|---|---|---|---|---|
| | | | XRD | XANES | |
| H1 | As grown | CoO | 43.59 | 46.3 | 4.2502(3) |
| | | $Co_3O_4$ | 49.56 | 53.7 | 8.0635(2) |
| H2 | 300 °C | CoO | 33.16 | 35.9 | 4.2528(1) |
| | | $Co_3O_4$ | 65.16 | 64.1 | 8.0686(2) |
| H3 | 500 °C | CoO | 3.20 | 3.7 | 4.2561(4) |
| | | $Co_3O_4$ | 96.80 | 96.3 | 8.0697(3) |
| H4 | 800 °C | CoO | 0.0 | 0.0 | NA |
| | | $Co_3O_4$ | 100 | 100 | 8.0761(3) |

outward diffusion of Co is faster than the inward diffusion of O. It is also reported that even different phases of CoO (rocksalt or wurtzite) transform to spinel phase of $Co_3O_4$ in air during the oxidation with retention of the original crystal morphology [26]. High temperature annealing improves the crystallinity of the nanoparticles due to the rearrangement of cobalt cations and oxygen anions of CoO to the spinel $Co_3O_4$ phase.

To confirm the above qualitative results, quantitative phase composition analysis using the Linear Combination Fitting (LCF) method on XANES data has been done. LCF works on least square fit algorithm using the XANES spectra for selected standards to determine the composition of an unknown sample. The basic principle of this method is based on the additive nature of absorption from each chemical state or species in the samples. The LCF method fits the unknown sample as a linear combination of standards according to their valance states. The pure phase of CoO (H0) and $Co_3O_4$ (H5) are used as standards. The normalized $\mu(E)$ data obtained for all the samples have been fitted by the linear combination of the normalized $\mu(E)$ data of standard samples. The experimental data and the best fit obtained are presented in Fig. 3. The goodness-of-fit are judged by $R$ (residual) and chi-square values. Percentages of the phases in as grown and annealed samples are obtained from the fit and are tabulated in Table 2. The phase compositions obtained through XANES data are compared with those obtained from Rietveld analysis on Synchrotron X-ray diffraction data (to be discussed in Section 3.4). These values are found to be nearly the same.

### 3.3. X-ray photoelectron spectroscopy (XPS)

XANES measurement (performed in transmission mode) described in Section 3.2 is a bulk sensitive measurement. In case of transition metal oxide nanoparticles, it is not uncommon to get a core shell structure; in which core and shell have different phases [27]. Therefore it is important to discuss surface characterization of as grown (H1) and annealed samples (H2–H4) using a surface sensitive technique like XPS [28]. Main peak for CoO and $Co_3O_4$ phases lie within very narrow range (within the instrumental resolution limit). Hence the two phases could not be distinguished based on their main peak positions. However, one can distinguish different phases (CoO and $Co_3O_4$) in case of cobalt oxide nanoparticle by noting the difference in the positions of the satellite peak with respect to the main peak. Satellite peak position for CoO is nearly 5–7 eV higher than its main peak, whereas, that for $Co_3O_4$ it is nearly 8–10 eV higher. It is also important to note that the satellite peak intensity in case of CoO is higher as compared to that for $Co_3O_4$ [[29,30] and references therein]. XPS spectra of as grown (H1) and annealed samples (H2–H4) are shown for Co 2p edge (Fig. 4a) and O 1s edge (inset in Fig. 4a). Peak analysis is carried out using carbon peak at 284.6 eV as reference point. Co 2p spectra for as grown sample (H1) show Co $2p^{1/2}$ and Co $2p^{3/2}$ main peaks at 795.2 eV and 779.9 eV respectively with broad satellite peaks. Occurrence of broad satellite peaks may be because of superposition of 2 or 3 peaks to be discussed later. Binding energies (BE) of both the main peaks are red shifted by ~0.4 eV with increase in the annealing temperatures (samples H2–H4). Further, separation between the satellite and the main peak positions increases with the increase in annealing temperature. The intensity of the satellite peaks also increases with increasing in annealing temperature indicating increase in $Co_3O_4$ concentration. No shake-up satellite peaks (in between the two main peaks) for as grown samples (H1) is observed indicating $Co^{3+}$ in octahedral cage on the surface of nanoparticles. Whereas, annealed samples show clear but subdued satellite peaks. The satellite peak for Co $2p^{1/2}$

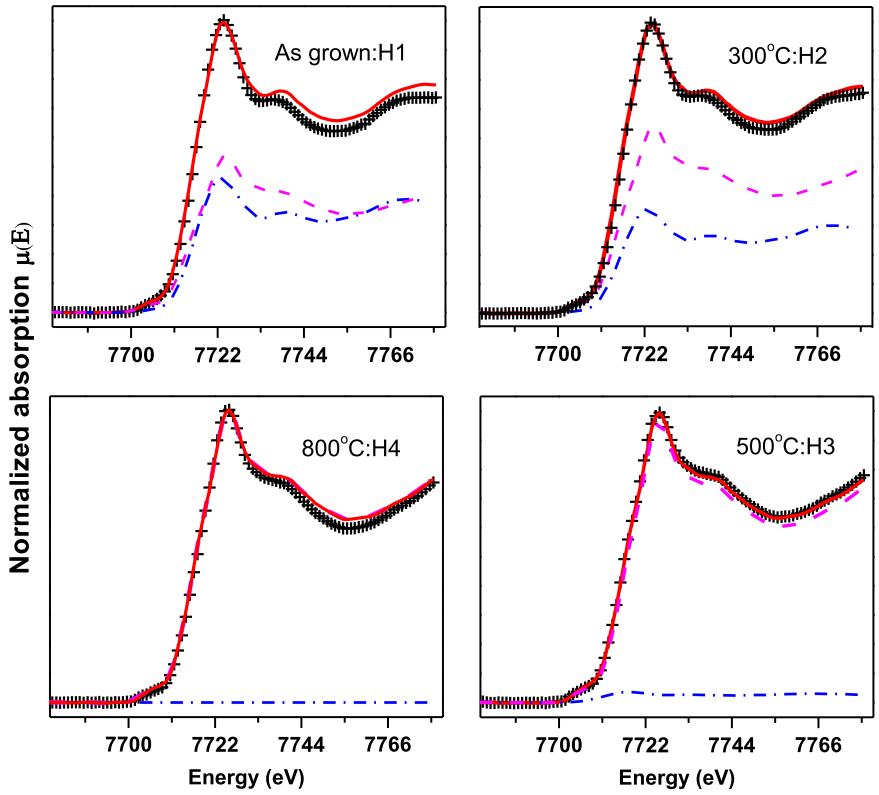


**Fig. 3.** Linear Combination Fitting (LCF) for all the samples H1–H4 using cobalt K-edge XANES spectra. Raw data points are shown by black (+) and solid lines (red) denote LCF fit to the data. Fractions of standards CoO (shown by blue dash dot) and $Co_3O_4$ (shown by magenta dash) are used for LCF. (For interpretation of references to color in this figure legend, the reader is referred to the web version of this article.)

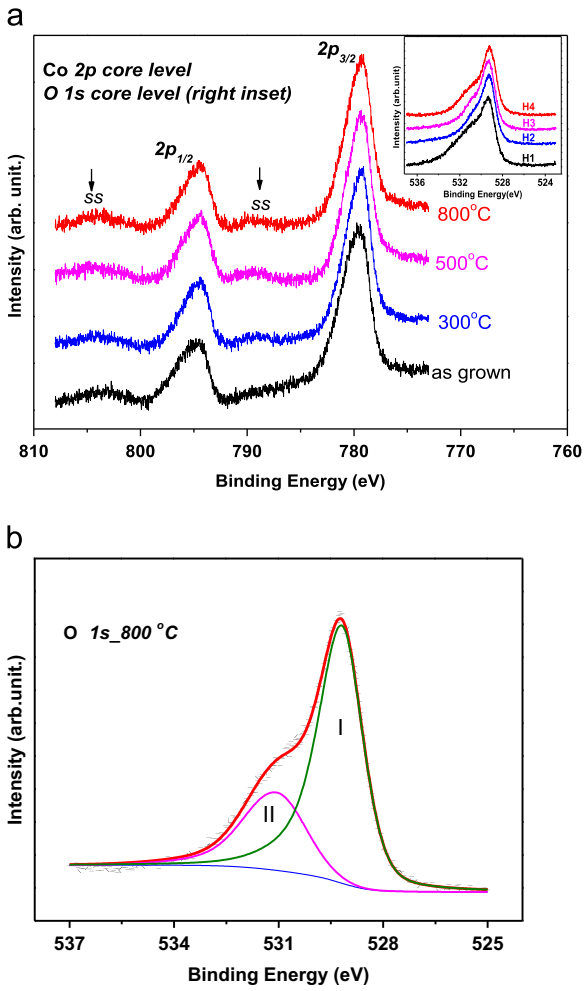


**Fig. 4.** (a) Normalized core level XPS spectra of Co 2p and O 1s (*right inset*) for all the samples (H1–H4). (b) Oxygen 1s XPS spectra of cobalt oxide nanoparticle sample H4 fitted with Shirley background and two Lorentzian–Gaussian peaks (I, II).

and Co $2p^{3/2}$ peaks are shifted by $(9.3 \pm 0.1)$ eV and $(10.2 \pm 0.1)$ eV respectively from their main peaks for sample H4. Further, the values of the peak shift increases slightly with the increase in annealing temperature. This clearly indicates that the concentration of $Co_3O_4$ phase increases with increase in annealing temperature. These results are in agreement with XANES results. The separation between the main and the satellite peaks (about 10 eV) are slightly higher than the values (8.5 eV ($p^{1/2}$) to 8.8 eV ($p^{3/2}$)) reported for bulk/thin film/epitaxial $Co_3O_4$ [31]. Satellite peaks are attributed to crystal field splitting for $Co^{2+}$ $3d^7$ energy states in tetrahedral crystal field environment. We believe that this is a significant result because it shows larger crystal field spitting for nanoparticles compared to that in the bulk. The separation between Co $2p^{1/2}$ and Co $2p^{3/2}$ main peaks lie within $15.3 \pm 0.1$ eV (Fig. 4a) for all the samples (H1–H4). This also suggests that the spin–orbit multiplet separation is not sensitive to ionic valence state of cobalt in the cobalt oxides [31].

Oxygen (O) 1s peaks for samples H2–H4 are the same at $529.3 \pm$ 0.1 eV. Based on O 1s binding energy we rule out any appreciable charging effect in our data and no manipulation in the energy axis has been done to nullify charging effect. The photoelectron spectral features of O 1s peak for the sample H4 at $\sim 529.3 \pm 0.1$ eV clearly indicates the presence of pure $Co_3O_4$ phase, in agreement with the XANES result. Analysis of O 1s core level XPS peak for all samples after removing the Shirley background and with minimum number of Gaussian–Lorentzian peaks is carried out using XPSPEAK 4.1 [32]. Oxide peak corresponds to $529.30 \pm 0.05$ eV position for all the samples (H1–H4). The second peak observed at $\sim 531.6$ eV is attributed to the adsorbed hydroxyl group [29,30]. This peak shifts to slightly higher value in position and lower value in FWHM on annealing (H2–H4). The position (FWHM) value is: 530.63 eV (2.37) for H2, 530.82 eV (2.15) for H3 and 531.08 eV (1.99) for H4 and 531.06 eV (3.09) for as grown (H1) sample. A representative fit is shown in Fig. 4b for the sample H4. The intensity ratios (area under the peak) of the peak I and peak II are 0.81 (for H1), 1.13 (H2), 1.39 (H3) and 2.65 (H4). In the literature, there is some controversy regarding relative intensity of the two peaks (marked I and II in Fig. 4b). Bonnelle et al. [33,34] have reported a 1:1 intensity ratio of peak I: peak II for $Co_3O_4$, whereas Hirokawa et al. [35] observed only a weak intensity for peak II. For CoO, Bonnelle et al. observed a 2:1 ratio, whereas Kim et al. [31] and Pollak et al. [36] suggested less than 10% relative intensity of peak II. Most of the literature [31,35,36], however suggest decrease in relative intensity of peak II with increase in $Co_3O_4$ concentration. Therefore we can safely infer qualitatively that $Co_3O_4$ concentration increases and adsorbed hydroxyl group decreases with the increase in annealing temperature in agreement with XANES result.

### 3.4. Synchrotron X-ray diffraction (SXRD)

SXRD measurements have been performed to corroborate the quantitative phase compositions, obtained through XANES data analysis (Section 3.2). For that Rietveld refinement [37], a well known quantitative phase composition analysis technique [38] is used. Two phase (CoO and $Co_3O_4$) refinement for all the samples (H1–H4) is used initially. Composition, unit cell parameters, Wyckoff positions and peak profile parameters etc. have been used as the refinable parameters. The crystal symmetries are Fd3m ($Co_3O_4$) and Fm3m (CoO). In case of samples H1 and H2, we are not able to fit the data reasonably using two phase refinement. Some extra peaks have been observed in the XRD patterns for these two samples. These extra peaks correspond to Co metallic phase in the sample confirmed by JCPDS database (PDF # 150806).

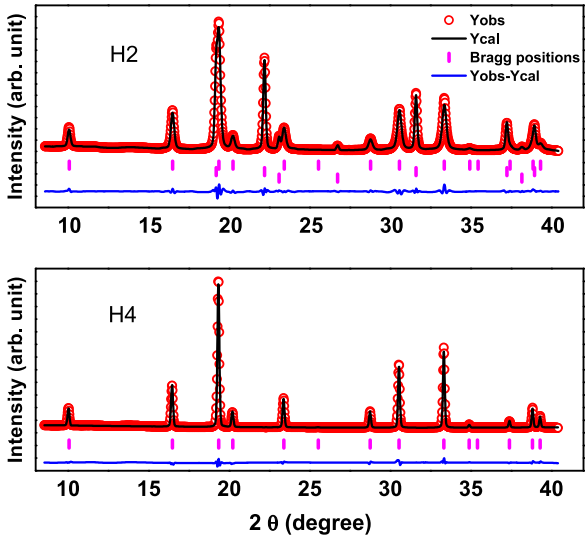


**Fig. 5.** Representative, Synchrotron X-ray diffraction patterns recorded at room temperature from cobalt oxide nanoparticle samples (here H2 and H4 only). Red dots represent the raw data, and solid black lines are the fit obtained by the Rietveld refinement. The blue and magenta line beneath the pattern records the Bragg positions and difference between the observed and calculated patterns respectively. (For interpretation of references to color in this figure legend, the reader is referred to the web version of this article.)

Variations particularly in samples H1 and H2 can be understood by three phase Rietveld refinement (Table 2). Co with space group Fm3m is used as the third phase. Analysis shows that Co metallic phase is present with concentration of ~6% and ~2% in samples H1 and H2 respectively. This is in agreement with the presence of weak type II magnetic contrast as observed in SEM for these two samples. This also leads to some discrepancy between SXRD and XANES results for these two samples (Table 2). A representative Rietveld refinement fit for samples H2 and H4 has been shown in Fig. 5 along with the quality of fit.

Phase compositions for all the samples obtained from Rietveld analysis suggests that as grown sample (H1) and sample annealed at 300 °C (H2) are in mixed phase of Co, CoO, and $Co_3O_4$. For samples H3 and H4, we have found that CoO phase oxidized to $Co_3O_4$ in agreement with XANES results. Rietveld refinement results for all the samples are summarized in Table 2 along with the composition obtained from XANES analysis. We find reasonably good agreement (within 4%) between the compositions obtained from SXRD and XANES analysis. Table 2 shows a comparative study of all the samples (H1–H4) together with their refined cell parameters.

Quantitative phase compositions using Rietveld refinement (SXRD) and LCF (XANES) have been obtained. Both the methods are based on least square fit algorithm and require prior knowledge of the phases that exist in the sample. In the case of Rietveld refinement one needs complete crystallographic information i.e. Wyckoff positions (fractional coordinates) of atom in the unit cell and unit cell parameters etc. for the corresponding phases. However, in case of LCF, only standard XANES spectra of all the phases are required. These standard spectra are used as combination for an unknown sample to obtain the composition depending on their chemical state. Therefore, XANES can also be a useful technique for quantitative phase composition analysis in the case of samples having complex structure, for which crystallographic information are not readily available.

## 4. Conclusions

Qualitative analysis of XANES spectra of as grown and isochronally annealed samples of cobalt oxide nanoparticles show that as grown together with annealed at 300 °C samples are in mixed phase of CoO and $Co_3O_4$. The phase concentration of $Co_3O_4$ increases with increase in annealing temperature at ambient. Quantitative XANES analysis shows $Co_3O_4$ phase concentration increases from ~49% in sample H1 to 100% for sample H4. These results have been corroborated with Rietveld analysis on SXRD data. The composition obtained from the two methods is in reasonably good agreement. This suggests that XANES can be effectively used to study composition of mixed phase samples. In addition, transition energies for $1s \rightarrow 3d$, $1s \rightarrow 4s$ and $1s \rightarrow 4p$ transitions have been estimated from XANES spectra. Surface characterization using XPS at Co 2p and O 1s edges show that surface are sensitive to annealing. On annealing adsorbed hydroxyl group decreases. XPS results indicate the increase in $Co_3O_4$ phase concentration on the surface, in agreement with the phase concentration changes for the bulk. Moreover, crystal field splitting is found to be larger in nanoparticles as compared to that in the bulk.

## Acknowledgments

The authors acknowledge Dr. N.P. Lalla and Ashok Kumar for their help during Rietveld analysis on SXRD data, Dr. Chandrachud Mukherjee for gold coating, and A.D. Vadikar for performing XPS measurements. We thank Dr. Haranath Ghosh for carefully reading of the manuscript. Mr. Harishchandra Singh wishes to acknowledge Homi Bhabha National Institute, India for providing research fellowship during his PhD work.

## References

[1] Peter Day, Noel S. Hush, Robin J.H. Clark, Philos. Trans. R. Soc. A 366 (2008) 195–204;
J.M.D. Coey, M. Viret, S. von Molnar, Adv. Phys. 48 (1999) 167–293;
T. Wu, et al., Phys. Rev. Lett. 86 (2001) 5998–6001;
Jin Wang, Shaomin Tian, Robby A. Petros, Mary E. Napier, Joseph M. De Simone, J. Am. Chem. Soc. 132 (2010) 11306–11313.
[2] X. Xie, Y. Li, Z.Q. Liu, M. Haruta, W. Shen, Nature 458 (2009) 746–749.
[3] F. Jiao, H. Frei, Angew. Chem. Int. Ed. 48 (2009) 1841–1844.
[4] H.K. Lin, H.C. Chiu, H.C. Tsai, S.H. Chien, C.B. Wang, Catal. Lett. 88 (2003) 169–174;
T. Zhu, J. Luo, J.K. Liang, G.H. Rao, J.B. Li, J.Y. Zhang, Z.M. Du, Physica B 403 (2008) 3141–3145.
[5] T. Maruyama, S. Arai, J. Electrochem. Soc. 143 (1996) 1383–1386.
[6] G.B. Smith, A. Ignatiev, G. Zajac, J. Appl. Phys. 51 (1980) 4186–4196.
[7] W. Li, L. Xu, J. Chen, Adv. Funct. Mater. 15 (2005) 851–857.
[8] Elena Papisa, Federica Rossi a, Mario Raspantib, Isabella Dalle-Donnec, Graziano Colomboc, Aldo Milzanic, Giovanni Bernardinia d, Rosalba Gornatia, Toxicol. Lett. 189 (2009) 253–259.
[9] Hu. Linhua, Peng Qing, Li Yadong, J. Am. Chem. Soc. 130 (2008) 16136–16137;
G. Fierro, G. Ferraris, R. Dragone, M. Lo Jacono, M. Faticanti, Catal. Today 116 (2006) 121–131;
M. Wojciechowska, W. Przystajko, M. Zielinski, Catal. Today 119 (2007) 338–341.
[10] W.L. Roth, J. Phys. Chem. Solids 25 (1964) 1;
Y. Ikedo, J. Sugiyama, H. Nozaki, H. Itahara, et al., Phys. Rev. B 75 (2007) 054424–054428.
[11] Babasola Ajiboye, Olalekan O. Akinremi, Astrid Jürgensen, Soil Sci. Soc. Am. J. 71 (2007) 1288–1291.
[12] R.K. Gupta, A.K. Sinha, B.N. Raja Sekhar, A.K. Srivastava, G. Singh, S.K. Deb, Appl. Phys. A 103 (2011) 13–19;
A.K. Sinha, R.K. Gupta, S.K. Deb, Appl. Phys. A 108 (2012) 607–611.
[13] A.K. Bakshi, S.N. Jha, L. Olivi, D.M. Phase, R.K. Kher, D. Bhattacharyya, Nucl. Instrum. Methods Phys. Res. B 264 (2007) 109–116.
[14] A.K. Sinha, A. Sagdeo, Pooja Gupta, Anuj Upadhyay, Ashok Kumar, M.N. Singh, R.K. Gupta, S.R. Kane, A. Verma, S.K. Deb, J. Phys.: Conf. Ser. 425 (2013) 072017.
[15] Gurnam Singh, Abdurahim, A. Banerji, et al., Proceedings of Indian Particle Accelerator Conference, 2006, pp. 94.
[16] A.P. Hammersley, S.O. Svensson, A. Thompson, Calibration and correction of spatial distortions in 2D detector systems, Nucl. Instrum. Methods A 346 (1994) 312–321.
[17] E.P. Bertin, Principles and Practice of X-ray Spectrometric Analysis, Plenum Press, New York, 1970.
[18] B.K. Teo, D.C. Joy, EXAFS Spectroscopy Techniques and Applications, Plenum Press, New York, 1981.
[19] J. Stöhr, NXAFS Spectroscopy, Springer Series in Surface Science, Springer, New York, 1992.
[20] Takashi Yamamoto, X-ray Spectrom. 37 (2008) 572–584.
[21] H. Fricke, Phys. Rev. 16 (1920) 202–215.
[22] M. Brown, R.E. Peierls, E.A. Stern, Phys. Rev. B 15 (1977) 738.
[23] B. Ravel, M. Newville, J. Synchrotron Radiat. 12 (2005) 537–541.
[24] Alain Manceau, Matthew A. Marcus, Sylvain Grangeon, Am. Mineral. 97 (2012) 816–827.
[25] Frank de Groot, Gyorgy Vanko, Pieter Glatzel, J. Phys. Condens. Matter 21 (2009) 104207;
D. Bazin, I. Kovacs, L. Guczi, P. Parent, C. Laffon, F. de Groot, O. Ducreux, J. Lynch, J. Catal. 189 (2000) 456–462.
[26] Don-Hyung Ha, Liane M. Morea, et al., J. Phys. Chem. C 117 (2013) 14303–14312;
Ki Min Nam, Jae Ha Shim, Dong-Wook Han, et al., Chem. Mater. 22 (2010) 4446–4454.
[27] J.P. Liu, E. Fullerton, O. Gutfleisch, D.J. Sellmyer (Eds.), Nanoscale Magnetic Materials and Applications, XX, Springer, Berlin, 2009. (732pp., 100 illus).
[28] T.J. Chuang, C.R. Brundle, D.W. Rice, Surf. Sci. 60 (1976) 286.
[29] S.C. Petitto, M.A. Langell, J. Vac. Sci. Technol. A 22 (2004) 1690–1696.
[30] C.A.F. Vaz, D. Prabhakaran, E.I. Altman, V.E. Henrich, Phys. Rev. B 80 (2009) 155457.
[31] K.S. Kim, Phys. Rev. B 11 (1975) 2177–2185.
[32] R.W.M. Kwok. Available for downloading at: ⟨http://www.phy.cuhk.edu.hk/~surface/xpspeak/⟩.
[33] J. Grimblot, A. D'Huysser, J.P. Bonnelle, J.P. Beauflis, J. Electron Spectrosc. 6 (1975) 71.
[34] J.P. Bonnelle, J. Grimblot, A. D'Huysser, J. Electron Spectrosc. 7 (1975) 151.
[35] K. Hirokawa, F. Honda, M. Oku, J. Electron Spectrosc. 6 (1975) 333–345.
[36] R.A. Pollak (Ph.D. thesis), Lawrence Berkeley Laboratory Report LBL-1299, 1972.
[37] J. Rodriguez-Carvajal, Physica B 192 (1993) 55–69.
[38] D.L. Bish, S.A. Howard, J. Appl. Crystallogr. 21 (1988) 86–91.